Parallel Interleaved VSCs: Influence of the PWM Scheme on the Design of the Coupled Inductor

Gohil, Ghanshyamsinh Vijaysinh; Bede, Lorand; Maheshwari, Ram Krishan; Teodorescu, Remus; Kerekes, Tamas; Blaabjerg, Frede

Published in:
Proceedings of the 40th Annual Conference of the IEEE Industrial Electronics Society, IECON 2014

DOI (link to publication from Publisher):
10.1109/IECON.2014.7048730

Publication date:
2014

Document Version
Early version, also known as pre-print

Parallel Interleaved VSCs: The Influence of the PWM Scheme on the Design of the Coupled Inductor

Ghanshyamsinh Gohil, Lorand Bede, RamKrishan Maheshwari, Remus Teodorescu, Tamas Kerekes, Frede Blaabjerg
Department of Energy Technology
Aalborg University, Denmark
gvg@et.aau.dk

***Abstract*—The line current ripple and the size of the dc-link capacitor can be reduced by interleaving the carriers of the parallel Voltage Source Converters (VSCs). However, the interleaving of carriers introduces circulating current between VSCs, and it should be suppressed. To limit the circulating current, magnetic coupling between the interleaved legs is provided by means of the Coupled Inductor (CI). The design of CI is strongly influenced by the pulsewidth modulation (PWM) scheme used. The analytical model to evaluate the flux-linkage in CI is presented in this paper. The maximum flux density and the core losses being the most important parameters for CI design, they are evaluated for continuous PWM and discontinuous pulsewidth modulation (DPWM) schemes. The effect of each of these PWM schemes on the design of the CI is discussed in the detail. The simulation and experimental results are finally presented to validate the analysis.**

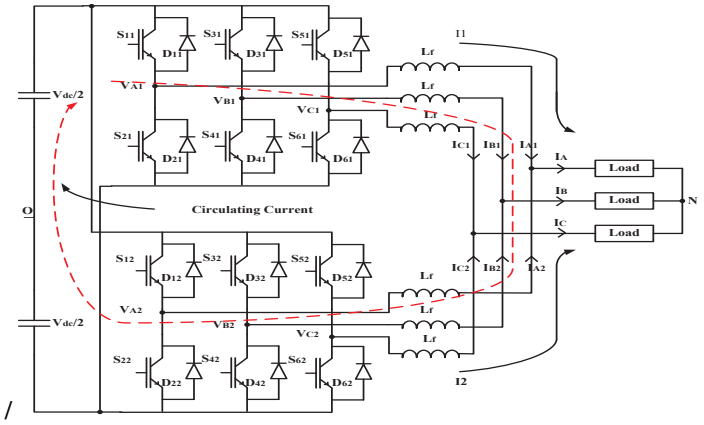

Fig. 1. Interleaved Parallel VSCs with common dc-link.

I. Introduction

The magnetic excitation in the core of the line filter inductor mainly has a line frequency component along with small high frequency ripple components. Reduction in the line filter inductor, by improving the line current quality leads to smaller filter and thus higher power density can be achieved. The line current quality can be improved by interleaving the carrier signals of the parallel Voltage Source Converters (VSCs) [1]–[6]. The discussion on the optimal interleaving angle to minimize the line current ripple is presented in [2]. The optimized PWM scheme involving multiple sequences and different interleaving angles to reduce the line current ripple is also presented [6]. The zone division plot showing the spatial regions within a sector, where a combination of certain switching sequence and interleaving angle results into lower rms current ripple in a switching cycle is also discussed.

However, interleaving of carriers leads to phase shifted pole voltages (measured with respect to the center point of the dc-link O in Fig. 1.) of the parallel interleaved legs. This results in circulating current between VSCs, and it should be limited in order to reduce the losses and the stresses in both active and passive components present in the circulating current path. The magnetic coupling between the interleaved parallel legs, by means of Couple Inductor (CI) is proposed [7]–[10] and the schematic is shown in Fig. 2(a). However, to achieve higher power density, the size of this additional circulating current filter should be reduced.

Neglecting the flux leakage between the coupled winding, the CI is only subjected to high frequency magnetic flux reversal determined by the switching frequency of the VSCs. Due to this high frequency operation core excitation, the size reduction can be achieved. Moreover, the maximum flux-density in the core should be kept high to utilize the core effectively. High frequency flux reversal along with the higher flux-density in the core results into more core losses. On the other hand, limited surface area is available for heat dissipation, if the design is performed with an objective to reduce the size of the CI. This may lead to thermally limited design. As the core losses also depend on the peak flux density, the design of the thermally limited inductor can be realized by either decreasing the peak flux density in the core or by providing more cooling. Both of these options lead to reduced power density.

The core losses depend on the peak flux density and the rate of change of flux density. Both of these parameters are strongly influenced by the PWM method used. The peak flux density in the core of CI for different PWM scheme is discussed in [9] and modulation method to reduce the flux in CI is also proposed. However, discussion on the core losses is not given, which is an important factor in determining the size of

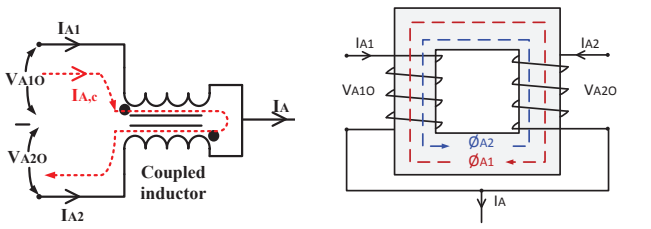

Fig. 2. Coupled inductor. (a) schematic for phase A, (b) physical arrangement of CI.

the thermally limited magnetic component, and it should be considered carefully for proper design of the CI.

The CI is a preferred solution to suppress the circulating current in parallel interleaved VSCs and the effect of the carrier based PWM schemes on the design of the CI is analyzed in this paper. The core experiences high frequency flux reversal and small size can be achieved. However due to the small size, the surface area available for heat dissipation is limited. The effect of the PWM scheme on the parameters affecting the core is discussed. Moreover, an analytical method to evaluate the maximum flux-density and losses in the CI for different PWM schemes is presented. The basic operation of the CI is discussed in Section II. The effect of the switching sequences on the flux density in the magnetic core of CI is presented in Section III. The influence of the flux density pattern on the design of the CI is presented in Section IV. In Section VI, the simulation results and the experimental results are finally presented to validate the analysis.

II. Coupled Inductor

The instantaneous difference in pole voltages of the interleaved legs of the parallel VSCs results into the circulating current. Thus, the individual leg current (I_{A1} and I_{A2}) carries circulating current in addition to the line current, and it can be decomposed into two components given as

$$\begin{aligned} I_{A1} &= I_{A1,l} + I_{A,c} \\ I_{A2} &= I_{A2,l} - I_{A,c} \end{aligned} \tag{1}$$

where, $I_{A1,l}$ and $I_{A2,l}$ are the components of the phase currents contributing to the resultant line current, and $I_{A,c}$ is the circulating current component. Assuming ideal VSCs and neglecting the effect of the hardware/control asymmetry, the current components contributing to the line current of the VSCs are considered equal, and the resultant line current is given as

$$I_A = 2I_{A1,l} = 2I_{A2,l} \tag{2}$$

The circulating current between the VSCs is

$$I_{A,c} = \frac{I_{A1} - I_{A2}}{2} \tag{3}$$

The magnetic coupling between the parallel interleaved legs provided by CI is used to suppress the circulating current, and it is discussed below.

The schematic of the coupled inductor is shown in Fig. 2(a), and one of the possible physical arrangements of the CI is depicted in Fig. 2(b). The flux linkage in CI is given as

$$\lambda_A(t) = \lambda_{A1}(t) + \lambda_{A2}(t) = \int (V_{A1O} - V_{A2O})dt \tag{4}$$

where V_{A1O} and V_{A1O} are the pole voltages measured with respect to the fictitious dc-link mid-point O, as shown in Fig. 1. The flux density in the core is given as

$$B_A(t) = \frac{1}{2NA_c} \int (V_{A1O} - V_{A2O})dt \tag{5}$$

where N is the number of turns and A_c is the core cross-sectional area. The maximum flux density and the core losses are the important parameters to consider in the design of the CI. From (5), it can be inferred that the flux density depends on the time integral of pole voltage differences, which in turn depends on the dc-link voltage, the interleaving angle,the modulation index, and the PWM scheme used. Therefore, the effect of PWM schemes on the design of CI is analyzed in following section.

III. Pulsewidth Modulation Schemes and their Effect on the Coupled Inductor Design

The reference space vector $\vec{V}_{ref}$ is sampled, and it's magnitude (V_{ref}) and angle (ψ) information is used for the selection of the two adjacent active state vectors along with zero vectors to synthesize the $\vec{V}_{ref}$ [11]–[13]. The respective dwell time of active vectors is chosen to maintain volt-sec balance. Let T_1, T_2, and T_z be the time during which the vectors $\vec{V}_1$, $\vec{V}_2$, and $\vec{V}_0/\vec{V}_7$ are applied respectively and it is given by

$$T_1 = \frac{2}{\sqrt{3}} \frac{|\vec{V}_{ref}|}{V_{dc}} T_s \sin(60° - \psi) \tag{6a}$$

$$T_2 = \frac{2}{\sqrt{3}} \frac{|\vec{V}_{ref}|}{V_{dc}} T_s \sin(\psi) \tag{6b}$$

$$T_z = T_s - T_1 - T_2 \tag{6c}$$

The time during which the zero vector is applied can be written as

$$\begin{aligned} T_z &= K_z T_0 + (1 - K_z) T_7 \\ &where,\ 0 \leqslant K_z \leqslant 1 \end{aligned} \tag{7}$$

Different modulation possibilities exist with variation in the parameter K_z [12]. $K_z = 0.5$ results into a classical center aligned SVM. Similarly, DPWM sequences can be generated by choosing the appropriate value of K_z. The SVM, DPWM1 (60°clamp), DPWM2 and DPWM3 (30°) clamp are considered for comparison [12]–[14] and discussed in following subsections.

A. The Center-aligned Space Vector Modulation

The opposite polarity zero vectors are applied at the same time for a duration of $T_z/4$. For a low modulation indices, the duty ratio of the zero vectors is dominant. As a result, the CI is subjected to more flux-linkage at lower modulation indices. In a thermally limited CI design, higher core losses due to

TABLE I
SVM: FLUX DENSITY DESCRIPTION IN A HALF SWITCHING CYCLE USING PIECEWISE LINEAR EQUATIONS

PWM scheme	Sub-sector	Peak flux density B_p	Flux density $B(t)$
SVM	$0° \leq \psi \leq 90°$	$B_p = \frac{V_{dc}(T_z)}{8NA_c}$	$B(t) = \frac{4B_p}{T_z}t$ for $0 \leq t \leq \frac{T_z}{4}$ $B(t) = B_p$ for $\frac{T_z}{2} \leq t \leq (\frac{T_s}{2} - \frac{T_z}{4})$ $B(t) = B_p - \frac{4B_p}{T_z}[t - (\frac{T_s}{2} - \frac{T_z}{4})]$ for $(\frac{T_s}{2} - \frac{T_z}{4}) \leq t \leq \frac{T_s}{2}$

TABLE II
DPWM1: FLUX DENSITY DESCRIPTION IN A HALF SWITCHING CYCLE USING PIECEWISE LINEAR EQUATIONS

Sub-sector	$\vec{V}_{ref}$ position	Peak flux density B_p	Flux density $B(t)$
$0° \leq \psi \leq 30°$	-	$B_p = 0$	$B(t) = 0$
$30° \leq \psi \leq 60°$	$M\cos(30-\psi) \geqslant \frac{1}{\sqrt{3}}$	$B_p = \frac{V_{dc}T_z}{4NA_c}$	$B(t) = \frac{-2B_p}{T_z}t$, for $0 \leq t \leq \frac{T_z}{2}$ $B(t) = -B_p$, for $\frac{T_z}{2} \leq t \leq \frac{T_s-T_z}{2}$ $B(t) = -B_p + \frac{2B_p}{T_z}[t - (\frac{T_s-T_z}{2})]$, for $\frac{T_s-T_z}{2} \leq t \leq \frac{T_s}{2}$
	$M\cos(30-\psi) < \frac{1}{\sqrt{3}}$	$B_p = \frac{V_{dc}(T_1+T_2)}{4NA_c}$	$B(t) = \frac{-2B_p}{T_1+T_2}t$, for $0 \leq t \leq \frac{T_1+T_2}{2}$ $B(t) = -B_p$, for $\frac{T_1+T_2}{2} \leq t \leq \frac{T_s-T_1+T_2}{2}$ $B(t) = -B_p + \frac{2B_p}{T_1+T_2}[t - (\frac{T_s-T_1-T_2}{2})]$, for $\frac{T_s-T_1-T_2}{2} \leq t \leq \frac{T_s}{2}$
$60° \leq \psi \leq 90°$	$M\sin(60-\psi_s) \geqslant \frac{1}{\sqrt{3}}$	$B_p = \frac{V_{dc}(T_z+T_3)}{4NA_c}$	$B(t) = \frac{-2B_p}{T_z+T_3}t$, for $0 \leq t \leq \frac{T_z+T_3}{2}$ $B(t) = -B_p$, for $\frac{T_z+T_3}{2} \leq t \leq \frac{T_s-T_z-T_3}{2}$ $B(t) = -B_p + \frac{2B_p}{T_z+T_3}[t - (\frac{T_s-T_z-T_3}{2})]$, for $\frac{T_s-T_z-T_3}{2} \leq t \leq \frac{T_s}{2}$
	$M\sin(60-\psi_s) \geqslant \frac{1}{\sqrt{3}}$	$B_p = \frac{V_{dc}T_2}{4NA_c}$	$B(t) = \frac{-2B_p}{T_2}t$, for $0 \leq t \leq \frac{T_2}{2}$ $B(t) = -B_p$, for $\frac{T_2}{2} \leq t \leq \frac{T_s-T_2}{2}$ $B(t) = -B_p + \frac{2B_p}{T_z+T_3}[t - (\frac{T_s-T_2}{2})]$, for $\frac{T_s-T_2}{2} \leq t \leq \frac{T_s}{2}$

more flux-linkage at a lower modulation indices decreases the achievable power density. The flux density pattern is symmetrical in every quarter cycle of the fundamental, and can be described using piecewise linear equation as given in Table I. The peak flux-linkage $\lambda_{A,p}$ changes in every half switching cycle. As can be inferred from the flux density description given in Table I, the $\lambda_{A,p}$ is a function of the modulation index M and the reference space vector angle ψ, and the maximum value of the peak flux-linkage as a function of modulation index is given as

$$\lambda_A, pmax = \frac{1}{4}V_{dc}T_s \tag{8}$$

Although the maximum value of the peak flux-linkage is the same for all modulation indices, the flux-linkage pattern is different. The flux density in the CI for different modulation indices is shown in Fig. 3. The peak flux density in each half switching cycle is higher for lower modulation indices, and reduces with increase in the modulation index as evident from Fig. 3.

B. DPWM1: 60°Clamp

In a grid connected application, the grid current has a power factor close to unity and the use of 60° clamp PWM (DPWM1) leads to switching loss reduction [11], [13], [15]. The unmodulated period for each phase leg is arranged around the positive and negative peaks of the respective reference voltage. The switching losses are reduced since each phase leg is clamped in a region where the current is at its maximum value [14].

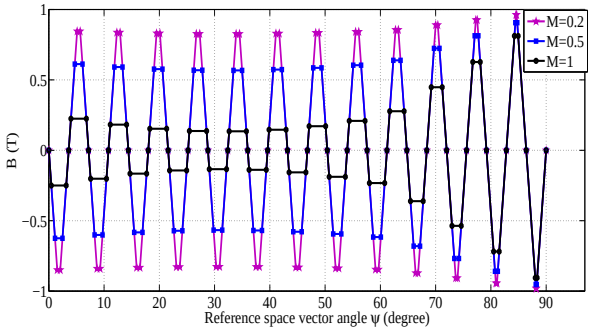

Fig. 3. The flux density in the CI core when SVM is used. The switching frequency is 2.5 kHz and maximum flux density in the core is restricted to 1 T.

The flux density in the CI depends on the magnitude and angle of the reference space vector $\vec{V}_{ref}$. The flux density can be described using piecewise linear equation as given in Table II. The flux density for the first quarter of the fundamental cycle is plotted in Fig. 4 for modulation index of 0.2, 0.5 and 1. The maximum peak flux-linkage varies with the modulation index, and it is given as

$$\lambda_{A,pmax} = \begin{cases} V_{dc}T_s(\frac{1}{\sqrt{3}}\frac{|\vec{V}_{ref}|}{V_{dc}}), & 0 \leq M < 1/\sqrt{3} \\ \frac{1}{4}V_{dc}T_s, & 1/\sqrt{3} \leq M < 2/\sqrt{3} \end{cases} \tag{9}$$

For modulation indices lower than $1/\sqrt{3}$, the maximum value of the peak flux density in case of DPWM1 is less than that of the SVM. However, for a modulation indices higher than

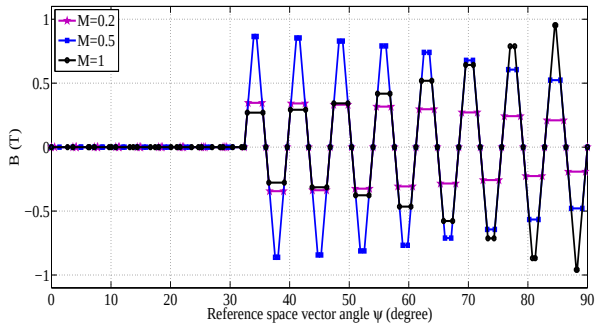

Fig. 4. The flux density in the CI core when DPWM1 is used. The switching frequency is 2.5 kHz and maximum flux density in the core is restricted to 1 T.

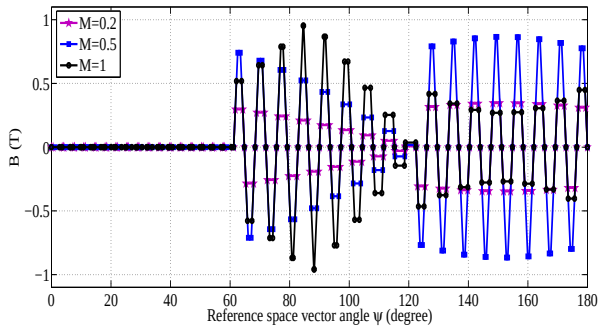

Fig. 5. The flux density in the CI core when DPWM2 is used. The switching frequency is 2.5 kHz and maximum flux density in the core is restricted to 1 T.

$1/\sqrt{3}$, the $\lambda_{A,pmax}$ for DPWM1 is the same as that of the SVM.

C. DPWM2: 30°Lagging Clamp

For a lagging power factor load, DPWM2 can results into lower core losses [16]. Due to the asymmetrical switching sequence in each subsector, the flux density no longer exhibits symmetry in a quarter period of the fundamental. Instead, the flux-density pattern is symmetrical in every half period of the fundamental cycle. Similar to DPWM1, the flux density in CI for DPWM2 can be also described by the piecewise linear equations. The flux density variation at different modulation indices is plotted as shown in Fig. 5. The maximum value of peak flux density $\lambda_{A,pmax}$ is same as that of the DPWM1, and can be described using (9).

D. DPWM3: 30°Clamp

In this PWM scheme, each phase leg is clamped to the opposite dc-link in each 60°segment. Different zero vectors are applied in each subsector. The flux density pattern is plotted

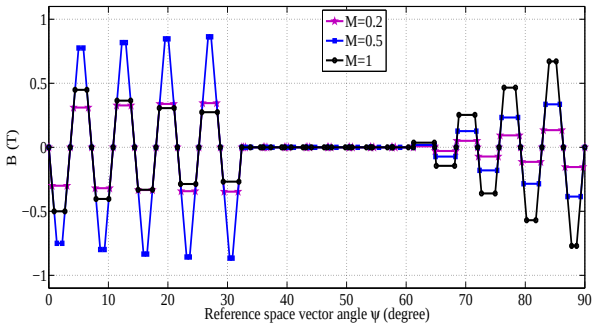

Fig. 6. The flux density in the CI core when DPWM3 is used. The switching frequency is 2.5 kHz and maximum flux density in the core is restricted to 1 T.

in Fig. 6. The peak flux-density $\lambda_{A,pmax}$ is given as

$$\lambda_{A,pmax} = \begin{cases} V_{dc}T_s(\frac{1}{\sqrt{3}}\frac{|\vec{\boldsymbol{V}}_{\boldsymbol{ref}}|}{V_{dc}}), \\ \qquad for\ 0 \leq M < 1/\sqrt{3} \\ \frac{1}{4}V_{dc}T_s, \\ \qquad for\ 1/\sqrt{3} \leq M < 2/3 \\ V_{dc}T_s(\frac{1}{2} - \frac{1}{2}\frac{|\vec{\boldsymbol{V}}_{\boldsymbol{ref}}|}{V_{dc}}), \\ \qquad for\ 2/3 \leq M < 4/(3+\sqrt{3}) \\ V_{dc}T_s(\frac{1}{2\sqrt{3}}\frac{|\vec{\boldsymbol{V}}_{\boldsymbol{ref}}|}{V_{dc}}), \\ \qquad for\ 4/(3+\sqrt{3}) \leq M < 2/\sqrt{3} \end{cases} \tag{10}$$

IV. Influence on the Coupled Inductor Design

The CI suppresses the circulating current by providing magnetic coupling between the interleaved parallel legs. Assuming tight magnetic coupling between the windings, the flux in the core has only high frequency components, which are concentrated around the odd multiple of the carrier frequency. The high frequency excitation could lead to significant size reduction of the CI. However, more losses due to the high frequency excitation may result into increased loss density, and considerable thermal management is required [17], [18]. In order to achieve higher power density, active cooling is preferred [17]. However, active cooling increases complexity and should be avoided.

The size of the CI can also be reduced by operating at higher flux density. However, it also leads to increased losses. Thus, the volume optimized design of CI may result into thermally limited design, where the maximum flux density in the core is determined by the heat dissipation capability of the CI [19], and not by the saturation flux density. For parallel interleaved VSCs, the PWM scheme has a strong influence on the maximum peak flux density and the losses in the CI. The variation in the maximum value of the peak flux-linkage with the modulation index for different PWM schemes [9] is plotted in Fig. 7. The maximum value of the peak flux linkage is the same in all schemes. however, the flux-linkage pattern is different. As a result, the core losses would be different in each

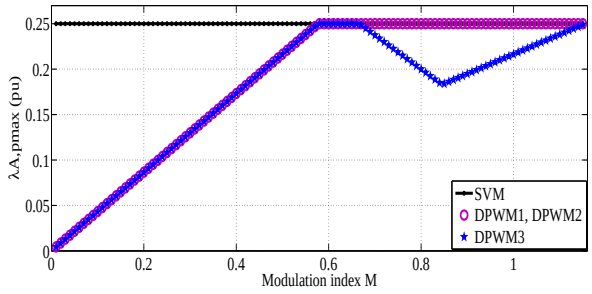

Fig. 7. The maximum peak flux linkage $\lambda_{A,pmax}$ variation with the modulation index. The flux-linkage is normalized with respect to the $V_{dc}T_s$.

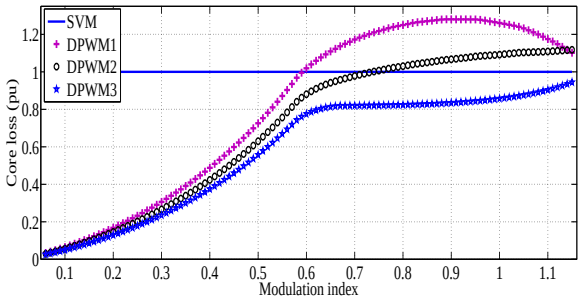

Fig. 8. The core losses in the CI for different PWM schemes. The core losses are normalized with respect to that of the SVM. The carrier frequency is taken to be the same in all cases.

of the schemes, which is an important factor in determining the size and the efficiency of the the CI, and it is discussed below.

The $\overrightarrow{\boldsymbol{V}}_{\boldsymbol{ref}}$ is sampled twice in a switching cycle, and the losses are evaluated for every half switching period. The flux density behavior in the half switching period can be described by the piecewise linear equations given in Table I and II for SVM and DPWM1 respectively.

The Improved Generalized Steinmetz Equation (IGSE) [20], [21] is used to calculate the core losses, and the core losses per unit volume is given as

$$P_v = \frac{1}{T}\int_0^T k_i \left|\frac{dB(t)}{dt}\right|^{\alpha} (\Delta B)^{\beta-\alpha} dt \tag{11}$$

where α, β and k_i are the constants determined by the material characteristics. Due to the quarter wave symmetry, the core losses are evaluated for each half switching cycle over a quarter period of the fundamental cycle. The average core loss over this period is given as

$$P_v = \frac{2}{\left(\frac{f_{sw}}{f_0}\right)} \sum_{k=1}^{\left(\frac{f_{sw}}{2f_0}\right)} \frac{2}{T_s} \int_0^{\frac{T_s}{2}} k_i (4B_{max} f_{sw})^{\alpha} (\Delta B_k)^{\beta-\alpha} dt \tag{12}$$

where f_0 is the fundamental frequency and f_{sw} is the switching frequency. The amorphous metal cores are considered, where the Steinmetz constants are $\alpha = 1.51$, $\beta = 1.74$ and $k_i = 0.622$.

To compare the PWM method independent of the design parameters, the volumetric losses in each of the DPWM scheme is normalized with respect to that of the SVM. Fig. 8 shows that the DPWM3 outperforms other schemes in terms of the core losses. All the DPWM schemes have lower core losses compared to SVM at lower modulation indices. The switching sequences of the DPWM2 are the same as the switching sequences of DPWM1 in one subsector 1 ($0° < \psi \leqslant 30°$), and switching sequences of DPWM3 in other subsector 2 ($30° < \psi \leqslant 60°$). Thus, the core losses of the DPWM2 is an average of the core losses of DPWM1 and core losses of DPWM3 as depicted in Fig. 8. For higher modulation indices, the DPWM1 has highest core losses, followed by the DPWM2 and SVM.

TABLE III
PARAMETERS FOR SIMULATION STUDY

Parameters	Simulation study
Switching frequency	2.5 kHz
DC-link voltage	680 V
Maximum flux density B_{max}	1 T
Window utilization factor K_w	0.5
RMS current in winding $I_{A,1(rms)}$	8 A
Current density J	2 A/m^2
Core material	Amorphous metal AMCC40
Core cross-sectional area A_c	$3.7\times10^{-4} m^2$
No. of turns N	92

V. Simulation and Experimental Results

The CI is designed using area product approach and the design outcome is given Table III. The area-product (A_p), which is the product of core cross-sectional area A_c and window area A_w is given as

$$A_p = A_c \times A_w = \frac{V_{dc,max} I_{A,1(rms)}}{4K_w J B_{max} F_s} \tag{13}$$

where $V_{dc,max}$ is the maximum dc-link voltage, $I_{A,1(rms)}$ is the rms current flowing through each winding, K_w is the window utilization factor and B_{max} is the maximum flux density. The magnetic model is implemented in PLECS and the simulated flux density is depicted in Fig. 9. The flux density pattern for all PWM schemes closely matches with the analysis presented in Section III. The flux density and the circulating current for SVM is plotted in Fig. 9(a) and 9(b), respectively. The simulation results are obtained with the modulation index of M=1. The core experiences the magnetic excitation only for 2/3 of the fundamental period for DPWM schemes as evident from Fig. 9. The maximum peak flux density in the CI is same in all PWM schemes with M=1 except the DPWM3. The DPWM3 has a lower maximum flux density for higher modulation indices as shown in Fig. 7. The circulating current is proportional to the flux density in the core as it is evident from the Fig. 9(a) and 9(b) and thus the circulating current is measured and used for comparison of PWM schemes in the experimental setup due to ease of the measurement.

Experimental measurements have been obtained to demonstrate the validity of the analysis presented in the paper.

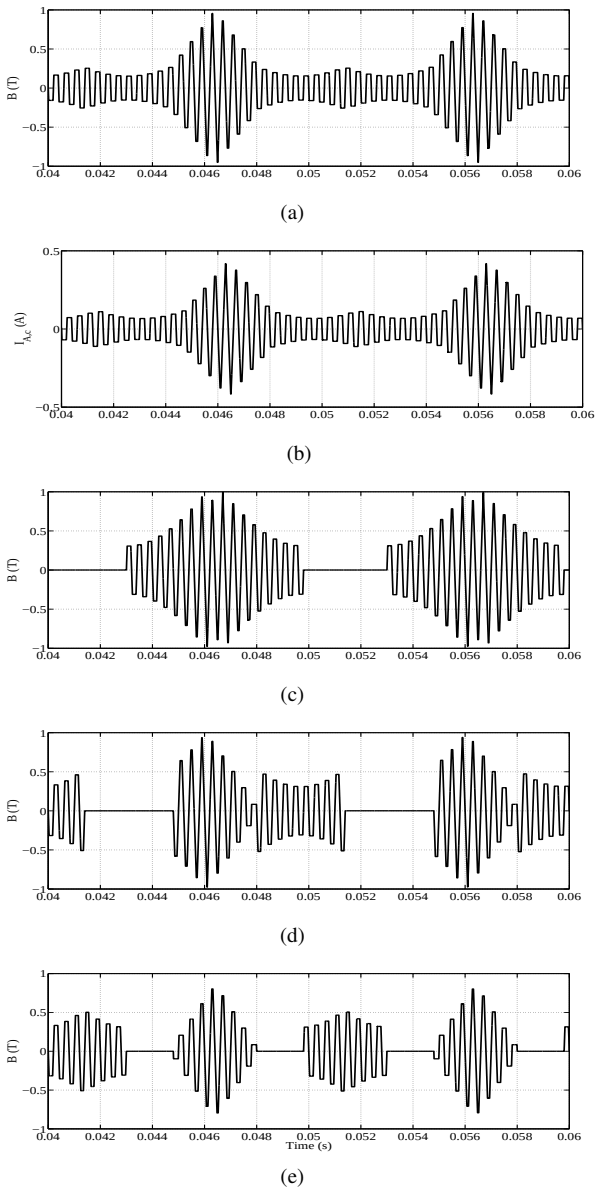

Fig. 9. Simulated flux density in the CI and the circulating current. (a) SVM: flux density, (b) SVM: circulating current, (c) DPWM1: flux density, (d) DPWM2: flux density, (e) DPWM3: flux density.

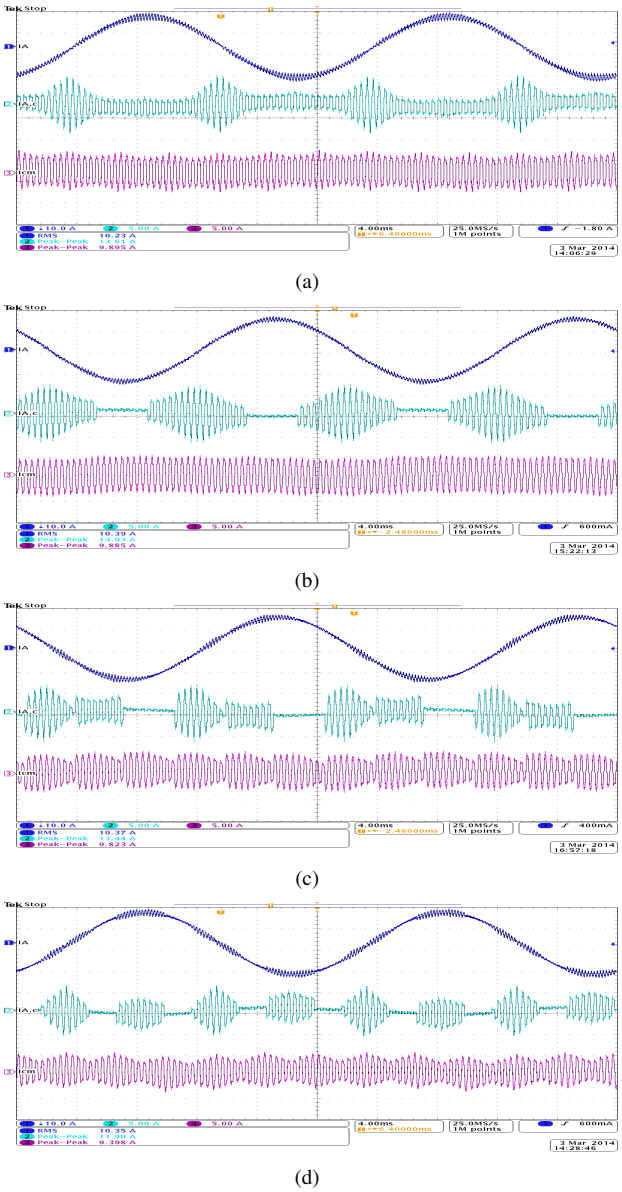

Fig. 10. Performance comparison of the PWM schemes: The modulation index M=1. (a) SVM: Ch1: Phase A line current, Ch2: Phase A circulating current ($2 \times I_{A,c}$), Ch3: common-mode circulating current ($3 \times I_{CM}$), (b) DPWM1, (c) DPWM2, (d) DPWM3.

The prototype has been built and the experiments have been performed on the setup and the schematic of the test setup is shown in fig. 1. The single phase inductors are used which will also introduce inductance in the circulating current path. This arrangement is adopted to simplify the measurement [9]. From Fig. 1, the dynamic behavior of the circulating current is given as

$$I_{A,c} = \frac{1}{2L_f} \int (V_{A1O} - V_{A2O})\, dt \tag{14}$$

From (4) and (14), it is clear that the circulating current in phase ($I_{A,c}$)is a replica of the flux linkage in the core, and the readings of $I_{A1} - I_{A2}$, which is equal to $2 \times I_{A,c}$ are obtained.

The dc-link voltage is set to 600 V. The carrier frequency is taken to be 2.5 kHz and the interleaving angle of 180°is chosen. The dead-time of 2 µs is used. The line filter inductor of 6.8 mH is used and resistive load is set to 20 Ω. The inductance in the circulating current path is 2×6.8 mH. The results for modulation index of 1 for different PWM schemes are given in Fig. 10.

The maximum value of the peak circulating current $I_{A,c}$ is measured for different PWM schemes. The modulation index is varied in full linear range. The peak value of circulation current is different in each half switching period and the highest value of the peak of $I_{A,c}$ is captured and given in Table IV. The circulating current is a replica of the flux-

linkage in the CI. The maximum value of the peak of the circulating current is the same in all of the PWM schemes. For SVM, a constant value of $I_{A,cmax}$ is observed over the entire modulation range, which is in agreement with the analysis presented in the Section III. The DPWM schemes have smaller $I_{A,cmax}$ for lower modulation indices, and the $I_{A,cmax}$ variation with modulation index matches with the analysis.

TABLE IV
COMPARISON: MAXIMUM VALUE OF PEAK OF $I_{A,c}$

M	$I_{A,cmax}$			
	SVM	DPWM1	DPWM2	DPWM3
0.1	3.55	0.79	0.81	0.84
0.2	3.52	1.46	1.47	1.47
0.3	3.50	2.09	2.07	2.02
0.4	3.55	2.68	2.67	2.63
0.5	3.50	3.23	3.19	3.20
0.6	3.48	3.72	3.72	3.79
0.7	3.48	3.63	3.63	3.71
0.8	3.42	3.55	3.42	3.27
0.9	3.40	3.50	3.42	2.82
1.0	3.40	3.48	3.36	2.97
1.1	3.36	3.48	3.36	3.24
1.15	3.38	3.39	3.37	3.37

VI. CONCLUSION

The influence of the PWM schemes on the design of the CI, used for the circulating current reduction in the parallel interleaved VSCs, is discussed. The carrier interleaving improves the line current quality, thus size of the line filter can be reduced. However, it requires additional circulating current filter. The design of this filter is strongly influenced by the PWM scheme used. The analytical model to evaluate the flux density in the CI is presented. The maximum value of the peak flux density for different PWM schemes is same, however the flux density pattern is different. This would results into different core losses. The core losses, being the important factor for proper thermal design of CI, it is also evaluated for each of the PWM schemes. The use of SVM incurs more core losses for lower modulation indices. The comparison also indicates that the use of DPWM3 results into lowest core losses in CI. Although the core is excited for 2/3 of the fundamental period in all DPWM schemes, the switching sequences involved in DPWM1 results into more flux linkage at higher modulation indices and thus incurs highest core losses for modulation indices higher than 0.6.

REFERENCES

[1] L. Asiminoaei, E. Aeloiza, P. N. Enjeti, and F. Blaabjerg, "Shunt active-power-filter topology based on parallel interleaved inverters," *IEEE Trans. Ind. Electron.*, vol. 55, no. 3, pp. 1175–1189, 2008.

[2] J. Prasad and G. Narayanan, "Minimization of Grid Current Distortion in Parallel-Connected Converters Through Carrier Interleaving," *IEEE Trans. Ind. Electron.*, vol. 1, no. c, pp. 1–1, 2013.

[3] S. Miller, T. Beechner, and J. Sun, "A comprehensive study of harmonic cancellation effects in interleaved three-phase vscs," in *Proc. IEEE Power Electronics Specialists Conference, 2007. PESC 2007.*, 2007, pp. 29–35.

[4] D. Zhang, F. Wang, R. Burgos, L. Rixin, and D. Boroyevich, "Impact of Interleaving on AC Passive Components of Paralleled Three-Phase Voltage-Source Converters," *IEEE Trans. Power Electron.*, vol. 46, no. 3, pp. 1042–1054, 2010.

[5] T. Bhavsar and G. Narayanan, "Harmonic analysis of advanced bus-clamping pwm techniques," *IEEE Trans. Power Electron.*, vol. 24, no. 10, pp. 2347–2352, 2009.

[6] X. Mao, A. Jain, and R. Ayyanar, "Hybrid interleaved space vector pwm for ripple reduction in modular converters," *IEEE Trans. Power Electron.*, vol. 26, no. 7, pp. 1954–1967, 2011.

[7] R. Hausmann and I. Barbi, "Three-phase multilevel bidirectional dc-ac converter using three-phase coupled inductors," in *Proc. IEEE Energy Conversion Congress and Exposition, 2009. ECCE 2009.*, Sept 2009, pp. 2160–2167.

[8] F. Forest, E. Laboure, T. Meynard, and V. Smet, "Design and comparison of inductors and intercell transformers for filtering of pwm inverter output," *IEEE Trans. Power Electron.*, vol. 24, no. 3, pp. 812–821, 2009.

[9] B. Cougo, T. Meynard, and G. Gateau, "Parallel Three-Phase Inverters: Optimal PWM Method for Flux Reduction in Intercell Transformers," *IEEE Trans. Power Electron.*, vol. 26, no. 8, pp. 2184–2191, Aug. 2011.

[10] B. Cougo, G. Gateau, T. Meynard, M. Bobrowska-Rafal, and M. Cousineau, "PD modulation scheme for three-phase parallel multi-level inverters," *IEEE Trans. Ind. Electron.*, vol. 59, no. 2, pp. 690–700, 2012.

[11] J. Kolar, H. Ertl, and F. C. Zach, "Influence of the modulation method on the conduction and switching losses of a pwm converter system," *IEEE Trans. Ind. Appl.*, vol. 27, no. 6, pp. 1063–1075, 1991.

[12] V. Blasko, "Analysis of a hybrid pwm based on modified space-vector and triangle-comparison methods," *IEEE Trans. Ind. Appl.*, vol. 33, no. 3, pp. 756–764, May 1997.

[13] A. Hava, R. Kerkman, and T. Lipo, "A high-performance generalized discontinuous pwm algorithm," *IEEE Trans. Ind. Appl.*, vol. 34, no. 5, pp. 1059–1071, 1998.

[14] D. G. Holmes and T. A. Lipo, *Pulse Width Modulation for Power Converters: Principles and Practice*. Hoboken, NJ: Wiley-IEEE Press, 2003.

[15] M. Depenbrock, "Pulse width control of a 3-phase inverter with nonsinusoidal phase voltages," in *Conf. Rec. IEEE Int. Semiconductor Power Conversion Conference*, 1997, pp. 399–403.

[16] A. Hava, R. Kerkman, and T. Lipo, "Simple analytical and graphical methods for carrier-based pwm-vsi drives," *IEEE Trans. Power Electron.*, vol. 14, no. 1, pp. 49–61, Jan 1999.

[17] G. Ortiz, J. Biela, and J. Kolar, "Optimized design of medium frequency transformers with high isolation requirements," in *Proc. 36th Annual Conference on IEEE Industrial Electronics Society, IECON 2010*, Nov 2010, pp. 631–638.

[18] R. Wrobel and P. Mellor, "Thermal design of high-energy-density wound components," *IEEE Trans. Ind. Electron.*, vol. 58, no. 9, pp. 4096–4104, Sept 2011.

[19] A. V. d. Bossche and V. C. Valchev, *Inductors and Transformers for Power Electronics*. Boca Raton, FL: CRC Press, 2004.

[20] K. Venkatachalam, C. Sullivan, T. Abdallah, and H. Tacca, "Accurate prediction of ferrite core loss with nonsinusoidal waveforms using only steinmetz parameters," in *Computers in Power Electronics, 2002. Proceedings. 2002 IEEE Workshop on*, 2002, pp. 36–41.

[21] J. Li, T. Abdallah, and C. Sullivan, "Improved calculation of core loss with nonsinusoidal waveforms," in *Industry Applications Conference, 2001. Thirty-Sixth IAS Annual Meeting. Conference Record of the 2001 IEEE*, vol. 4, 2001, pp. 2203–2210 vol.4.

[22] G. Narayanan and V. T. Ranganathan, "Analytical evaluation of harmonic distortion in pwm ac drives using the notion of stator flux ripple," *IEEE Trans. Power Electron.*, vol. 20, no. 2, pp. 466–474, 2005.

[23] G. Narayanan, H. Krishnamurthy, D. Zhao, and R. Ayyanar, "Advanced bus-clamping pwm techniquesbased on space vector approach," *IEEE Trans. Power Electron.*, vol. 21, no. 4, pp. 974–984, 2006.

[24] G. Narayanan, V. T. Ranganathan, D. Zhao, H. Krishnamurthy, and R. Ayyanar, "Space vector based hybrid pwm techniques for reduced current ripple," *IEEE Trans. Ind. Electron.*, vol. 55, no. 4, pp. 1614–1627, 2008.